EPJ Web of Conferences **333**, 01001 (2025) https://doi.org/10.1051/epjconf/202533301001
XLVI Symposium on Nuclear Physics 2025

Strong Electromagnetic Fields in Heavy Ion Collisions

C.A. Bertulani[1,2,3,*]

[1]Department of Physics and Astronomy, East Texas A&M University, Commerce, Texas, 75025, USA
[2]ExtreMe Matter Institute EMMI, GSI, Darmstadt, Germany
[3]Institut für Kernphysik, Technische Universität Darmstadt, Germany

Abstract. Photons play a pivotal role in both theoretical and applied physics, ranging from elementary particle studies to practical technologies. This article explores how ultra-peripheral collisions of heavy ions act as sources of nearly real photons, enabling the investigation of a wide range of photon-induced processes. By applying the equivalent photon approximation, one can study nuclear structure, QED phenomena, and potential new physics, all in a background-suppressed environment.

1 Virtual and real photons

The study of electromagnetic processes in high-energy nuclear physics has benefited significantly from the development of the Equivalent Photon Method (EPM), which originated from an idea proposed by Enrico Fermi in 1924 [1]. His pioneering approach suggested that the time-dependent electromagnetic field of a fast-moving charged particle could be represented as a flux of quasi-real photons. This concept, though initially classical, has been refined using the language of quantum electrodynamics (QED) and perturbation theory, making it applicable to a wide range of processes involving nuclei and particles.

In the context of ultra-relativistic heavy ion collisions, such as those occurring at the Relativistic Heavy Ion Collider (RHIC) or the Large Hadron Collider (LHC), the Lorentz-contracted electromagnetic fields of the nuclei become extremely intense. These fields interact at large impact parameters, allowing the nuclei to remain intact while exchanging energy and momentum via virtual photon interactions. This regime, known as ultra-peripheral collisions (UPCs), is ideal for applying the EPM because the electromagnetic interaction dominates over hadronic contributions, which are suppressed by the large distance between the colliding nuclei.

The central premise of the EPM is to replace the time-dependent electromagnetic field with a distribution of equivalent photons. The interaction of these photons with a target can then be treated as if the photons were real. For each electric or magnetic multipolarity of the interaction, denoted by E or M, and characterized by angular momentum L, one defines an equivalent photon number density $n_{E/M,L}(\omega)$ as a function of the photon energy ω. The total cross section for a process can then be expressed as [2, 3]:

$$\sigma = \sum_{E/M,L} \int \frac{d\omega}{\omega} n_{E/M,L}(\omega) \sigma_{\gamma}^{(E/M,L)}(\omega), \tag{1}$$

*e-mail: carlos.bertulani@etamu.edu

where $\sigma_\gamma^{(E/M,L)}(\omega)$ is the cross section for the real photon process at energy ω.

The photon number $n_{E/M,L}(\omega)$ encapsulates the kinematic and dynamic aspects of the colliding system. It depends on the Lorentz factor γ of the projectile, the impact parameter b, the nuclear charge Z, and the transition multipolarity. For practical calculations, one integrates over all possible impact parameters larger than a minimum value $b_{\min}$ to exclude overlapping configurations where hadronic interactions may occur. The result is a spectrum of equivalent photons that can be used to compute cross sections for a wide variety of processes.

A key advantage of this approach is that it allows one to leverage tabulated or experimentally measured photoabsorption cross sections for processes such as nuclear excitation, particle production, and meson photoproduction. It also enables theoretical predictions based on model-dependent photonuclear reaction mechanisms. Examples include dipole excitations in stable and exotic nuclei, Coulomb excitation of low-lying collective states, and the production of vector mesons in coherent photon-nucleus interactions. It plays a critical role in understanding photon-photon and photon-gluon fusion mechanisms, contributing to our knowledge of QCD dynamics.

Attention is often directed toward the regime of high energies, where the interaction cross section can be approximated by

$$\sigma \simeq \sum_{E/M,L} \int \frac{d\omega}{\omega} n(\omega) \sigma_\gamma^{(E/M,L)}(\omega) = \int \frac{d\omega}{\omega} n(\omega) \sum_{E/M,L} \sigma_\gamma^{(E/M,L)}(\omega) = \int \frac{d\omega}{\omega} n(\omega) \sigma_\gamma(\omega), \quad (2)$$

with the total real-photon cross section defined by $\sigma_\gamma = \sum_{E/M,L} \sigma_\gamma^{(E/M,L)}$.

Equations 1 and 2 are derived under the assumption that only first-order processes contribute [3]. However, the photon is not a simple point-like particle; it can fluctuate into various intermediate states via quantum loop effects. These fluctuations modify its wavefunction, leading to a superposition of bare and virtual components:

$$|\gamma\rangle \quad = \quad C_{bare} |\gamma_{bare}\rangle + C_{ee} \left|e^- e^+\right\rangle + \cdots + C_{qq} |q\bar{q}\rangle + C_\omega |\omega\rangle + C_\phi |\phi\rangle + C_\rho |\rho\rangle + \cdots \quad (3)$$

Due to its quantum numbers $J^P = 1^-$, the photon readily converts into neutral vector mesons such as ρ, ω, ϕ, or J/ψ through quark-antiquark fluctuations, consistent with the principles of the vector dominance model. Additionally, the photon is inherently multicomponent in energy space, some components are off-shell or virtual. It may undergo processes involving internal splitting, emission of constituent parts, transitions through intermediate hadronic states, or reabsorption cycles [4].

2 Coulomb dissociation and nuclear astrophysics

Coulomb dissociation is an indirect approach to study radiative capture reactions, particularly those of relevance to nuclear astrophysics [5]. In this method, a projectile nucleus with a cluster structure, or a bound nucleon plus a core, is exposed to the intense electromagnetic field of a high-Z target nucleus. The interaction, occurring at large impact parameters to suppress nuclear interactions, mimics photo-disintegration by causing the projectile to break apart. By analyzing the resulting fragments and their energy spectra, one can infer the inverse process cross section using detailed balance principles, i.e., in the reaction $a+A \longrightarrow b+c+A$:

$$\frac{d\sigma_C^{E/M,L}(\omega)}{d\omega d\Omega} = \frac{dn^{E/M,L}(\omega;\theta;\phi)}{d\omega d\Omega} \cdot \sigma_{\gamma+a\to b+c}^{E/M,L}(\omega). \quad (4)$$

Here, $dn^{E/M,L}/d\omega d\Omega$ dependens on the scattering angle $\Omega = (\theta, \phi)$ [5]. Time reversal relates the reaction cross section for $b + c \longrightarrow a + \gamma$ to $\sigma_{\gamma+a\to b+c}^{E/M,L}(\omega)$. This method provides a clean

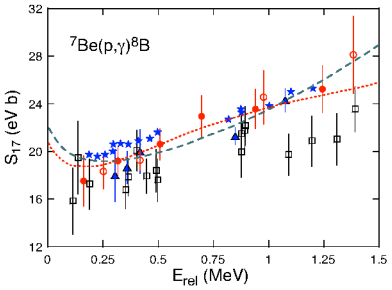

Figure 1. ^{7}Be(p,γ)^{8}B reaction at low energies. Calculations using the no-core shell-model [7] are shown by a dashed-line. The dotted line is a calculation using a resonant group method [8]. Experimental data are also shown [12–19].

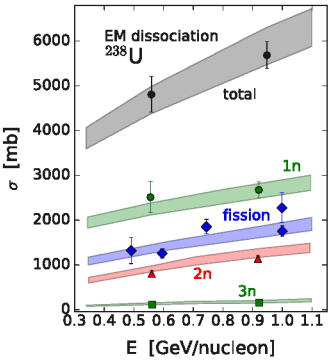

Figure 2. EM dissociation cross sections of ^{238}U projectiles. The projectiles fission (diamonds) and/or emit multiple neutrons (xn) [20–23]. Uncertainty bands for the numerical calculations are shown [24].

probe of neutron or proton capture rates, which are essential in nucleosynthesis pathways like the r-process or rp-process.

Experiments using this method have been successfully carried out at facilities such as RIKEN, GSI, and NSCL, targeting neutron-rich and proton-rich nuclei. Examples include the dissociation of ^{8}B, ^{11}Be, ^{15}C, and ^{19}C, providing critical information on astrophysical S-factors and nuclear halo structures. Due to the purely electromagnetic nature of the interaction, theoretical modeling is more reliable, with fewer uncertainties than hadronic reaction mechanisms. An example of application of this method is the ^{7}Be$(p,\gamma)^8$B reaction [6] as shown in Figure 1. The experimental data displayed as red dots were used the Coulomb dissociation method. See also Refs.[9–11].

The Coulomb dissociation method also serves to validate nuclear structure models, particularly those describing the continuum and resonant states. Its predictive power and ability to provide spectroscopic data on unbound states make it an indispensable tool in both fundamental nuclear physics and applied astrophysics. The contribution of nuclear breakup to the dissociation process has been studied and quantified in many works (see, e.g., Ref. [25]). Loosely-bound systems, or “halo nuclei" with small nucleon separation energies, are subjected to multiple-step higher-order effects including continuum-continuum couplings Ref. [25].

3 Excitation and decay of giant resonances

Giant resonances are collective excitations of the entire nucleus, where nucleons oscillate in a coherent manner under the influence of an external field. These modes are essential to understanding bulk nuclear properties, such as incompressibility, symmetry energy, and the effective interactions among nucleons. Among the most studied are the isovector giant dipole resonance (IVGDR), isoscalar monopole resonance (GMR), and quadrupole resonances.

Ultra-peripheral collisions offer a unique environment to excite giant resonances through the absorption of virtual photons [27, 33, 34]. As the electromagnetic field of a passing ion interacts with the nucleus, it can transfer energy sufficient to trigger these coherent modes. The excitation cross section depends on the strength function of the nucleus and the equivalent photon spectrum. For targets with large charge Z, the nuclear dissociation cross sections are much smaller than electromagnetic [3, 20–23]. In UPCs, their study has provided new

insights in studies of nuclear fission [28–30] and as a luminosity monitor in relativistic heavy-ion colliders [31, 32, 39] (see Figure 2).

The IVGDR is particularly sensitive to the neutron-to-proton ratio and is a key observable in determining the symmetry energy of nuclear matter. On the other hand, the GMR provides direct insight into nuclear compressibility, a parameter relevant to both finite nuclei and neutron star matter. Measurement of these modes requires detection of emitted gamma rays or decay particles following resonance excitation. The excitation of the double IVGDR in UPCs was proposed in Refs. [33, 34]. They were identified in experiments carried out at the GSI/Darmstadt laboratory [35, 36] using gamma-gamma coincidences from the decay of the decay of the double GDR (DGDR) [36], as well as by identifying neutron emission from its decay [35] (see Figure 3). The DGDR strength and width provide additional constraints of nuclear models for research on giant resonance [37, 38, 40]. This contributes significantly to the ongoing effort to constrain the nuclear equation of state.

4 Lepton pair production

One of the fundamental processes accessible in ultra-peripheral collisions is the creation of electron-positron pairs from the vacuum. This quantum electrodynamical (QED) phenomenon occurs when two colliding nuclei generate sufficiently strong electromagnetic fields to facilitate two-photon interactions. The process is described by lowest-order Feynman diagrams in QED and becomes increasingly probable with rising nuclear charge and beam energy. In its simplest form, pair production involves two virtual photons fusing to create a e^+e^- pair. The cross section scales approximately with the square of the nuclear charge and logarithmically with the Lorentz factor of the colliding ions, in the form [41–46]

$$\sigma_{e^+e^-} = \frac{28}{27\pi}(Z_1 Z_2 \alpha r_e)^2 \ln^3\left(\frac{\gamma}{2}\right). \tag{5}$$

The appearance of a triple logarithmic dependence originates from the interplay of several quantum electrodynamical mechanisms: (1) The momentum integration over the exchanged virtual photon between one nucleus and the e^+e^- pair yields a logarithmic term, as $\int dq^2/q^2 \sim \ln(q_{\max}/q_{\min}) \sim \ln\gamma$. (2) Since the produced pair tends to emerge at small angles relative to the beam axis, the angular integration gives another factor, $\int d\theta/\theta \sim \ln\gamma$. (3) The equivalent photon distribution from the opposing nucleus scales as $dN/d\omega \sim 1/\omega$, and the corresponding energy integration $\int_{\omega_{\min}}^{\omega_{\max}} d\omega/\omega \sim \ln\gamma$ introduces the third logarithm. These logarithmic contributions are characteristic features of QED in the ultra-relativistic domain, where boosted fields and collinear emission dominate the dynamics. Higher-order corrections include multiple pair production, Coulomb distortion effects, and screening phenomena are also important [3, 47].

A straightforward model for evaluating multiple pair production was based on the assumption that the number of produced pairs follows a Poisson distribution as a function of impact parameter. In this approach, the probability of generating n e^+e^- pairs at a given b is expressed as [3]

$$P_{e^+e^-}(b) = \frac{[P_0(b)]^n}{n!}\exp\left[-P_0(b)\right], \tag{6}$$

where $P_0(b)$ denotes the single-pair production probability [3], calculated by

$$P_0(b) = \frac{14}{9\pi^2 b^2}(Z_1 Z_2 \alpha r_e)^2 \ln^2\left(\frac{\gamma}{2m_e b}\right), \tag{7}$$

which applies within the interval $1/m_e < b < \gamma/m_e$ [3]. Several studies have extended this analysis to account for final-state effects in processes involving multiple pairs [48–51].

Measurements performed with the STAR detector at RHIC [52], and later by CMS at CERN [53], provided empirical support for these quantum electrodynamics-based predictions. The formation of other lepton or meson pairs via photon fusion, such as $\gamma\gamma \to \mu^+\mu^-$, $\gamma\gamma \to \pi^+\pi^-$, and $\gamma\gamma \to W^+W^-$, is also relevant, as shown in theoretical results from Refs. [3, 47, 54], and later corroborated [3, 3, 39, 54]. The formulas presented above are applicable to $\mu^+\mu^-$, $\pi^+\pi^-$, and $\tau^+\tau^-$ production under the condition that $\gamma \gg 16$ for muons and $\gamma \gg 200$ for taus. For lower values of γ, modifications to the expressions become necessary [3].

Beyond electrons, heavy lepton pair production and even bound-free pair creation, where the electron is captured by one of the nuclei, have also been observed. These processes contribute to beam losses in accelerators and are of practical relevance in beam lifetime studies.

5 Anti-hydrogen and other exotic atoms

A notable application of ultra-peripheral collisions (UPCs) involves lepton pair production where the negatively charged lepton is subsequently captured by one of the colliding nuclei [3, 56, 57]. The cross section for such a process, specifically, when the electron is trapped in a K-shell orbital, can be approximated by [3]

$$\sigma_K = \frac{33}{20} Z_1^5 Z_2^5 \alpha^5 r_e^2 \ln\left(\frac{\gamma}{2}\right). \tag{8}$$

To account for electron capture into higher atomic shells, one must multiply this result by the factor $\sum_n 1/n^3 \approx 1.202$. For high-$Z$ systems, electron screening and wavefunction distortions alter these values significantly [3].

This mechanism was proposed as a pathway for producing antihydrogen at the LHC [58], and its experimental verification came in a landmark CERN experiment in 1996 [59]. Conducted at the Low Energy Antiproton Ring (LEAR), this effort involved collisions between protons and antiprotons, with the latter capturing positrons to form neutral anti-atoms. This represented the first successful production of antihydrogen in a laboratory setting, with 11 atoms recorded, an achievement widely covered in major news outlets including the New York Times [60].

A similar experiment performed at Fermilab [61] identified 57 antihydrogen events, which were consistent with earlier theoretical forecasts [56, 62]. Since then, anti-atom investigations have continued using ion trapping technologies to probe fundamental symmetries [63, 64]. The utility of UPCs extends beyond antihydrogen: processes leading to anti-deuterium, anti-tritium, and even anti-helium nuclei have been proposed [65]. UPCs also provide a potential source of exotic atoms, such as muonic or pionic atoms, formed via coherent photon exchange, as outlined in [57].

The concept of e^+e^- pair production accompanied by electron capture into atomic orbitals has also been suggested as a source of beam loss in high-energy colliders [3]. Early estimates predicted that beams of heavy ions could degrade within hours due to this effect at the LHC. These predictions have been substantiated by further theoretical analyses [66] and recent experimental confirmations [67].

Another compelling aspect of UPCs is the creation of bound e^+e^- states, positronium, in either ortho or para configurations. Theoretical descriptions for positronium and related bound states, including mesons viewed as $q\bar{q}$ systems, have been developed within the framework of quantum field theory [68]. Fusion of two or three photons in UPCs can give rise to such bound states, as explored in Refs. [69–71]. In total, six leptonic atoms are theoretically possible: (a) positronium (e^+e^-), (b) muonium (μ^+e^-), (c) dimuonium ($\mu^+\mu^-$), (d) tauonium

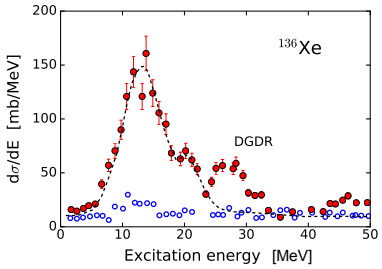

Figure 3. Giant resonances in ^{136}Xe observed in UPCs as a function of the excitation energy. A distinct peak at higher energy displays the Giant Dipole Resonance (DGDR) [35].

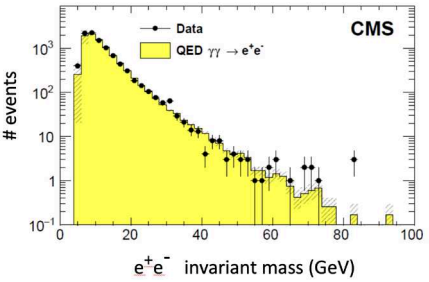

Figure 4. Number of events of e^+e^- pairs created in UPCs obtained with the CMS detector at the LHC (from Ref. [53]).

(τ^+e^-), (e) tau-muonium ($\tau^+\mu^-$), and (f) ditauonium ($\tau^+\tau^-$). Of these, only positronium, muonium, and the positronium molecule (dipositronium) have been observed so far [72–74].

Dimuonium is expected to be significantly more compact than either positronium or muonium, due to the heavier mass of the muons. Its unique mass scale renders it sensitive to potential phenomena beyond the Standard Model [75], particularly in time-like domains of QED. Detecting dimuonium would represent a major milestone in fundamental physics [76]. Production rates for dimuonium in UPC environments at the LHC have been calculated and found to be within measurable reach [77–80]. Moreover, recent work suggests that ditauonium might also be observed under similar conditions [82], with detection strategies relying on its displaced decay vertex and manageable background from dimuon events.

6 Photon-photon fusion

The process of elastic light-by-light scattering, $\gamma + \gamma \rightarrow \gamma + \gamma$, is mediated through rare quantum fluctuations, where a photon temporarily transforms into a particle-antiparticle pair. Due to the extremely small likelihood of such fluctuations, direct measurements using real photons remain impractical. In Ref. [3], we suggested that ultra-peripheral collisions (UPCs) could serve as an effective method for probing this phenomenon via the reaction $Z_1 + Z_2 \rightarrow Z_1 + Z_2 + \gamma + \gamma$. In this scenario, two virtual photons interact through a loop (box) diagram, resulting in the emission of two real photons. These calculations, based on Delbrück scattering formalism, involve considerable theoretical uncertainties [3]. The leading-order cross section for $\gamma^*\gamma^* \rightarrow \gamma\gamma$ in UPCs, particularly for high-energy photon final states, is given by [3]

$$\sigma_D \sim 2.54 \times 10^{-2} Z^4 \alpha^4 r_e^2 \ln^3\left(\frac{\gamma}{m_e R}\right), \tag{9}$$

where R denotes the radius of the heavy-ion nucleus. For Pb+Pb collisions at the LHC, the resulting cross section can be quite large, on the order of $\sigma_D \sim 50$ b. However, not all outgoing photons can be attributed unambiguously to this channel, as backgrounds, such as those from Bremsstrahlung, complicate the signal extraction. For photon energies $E_\gamma > m_\mu$, the cross section becomes significantly smaller, approximately $\sigma_D \sim 30$ nb [81].

Further theoretical studies expanded on these ideas, introducing alternative photon-photon scattering mechanisms including the VDM-Regge framework, two-gluon exchange models, and meson resonance contributions (see, for example, Refs. [83–87]). A major experimental milestone came with the ATLAS detector's observation of this elusive process at

the LHC (Figure 5) [88], lending credibility to prior theoretical models and opening the door to probing scenarios beyond the Standard Model (SM). Any measured cross section that exceeds the SM expectation could hint at the presence of new fundamental particles, such as axions [89–91].

7 Production of Mesons

To extend the Equivalent Photon Number (EPN) framework to include the formation of bound states in ultra-peripheral collisions, we proposed a method for calculating the production cross section of a generic particle X [3]. The photon-photon fusion cross section can be written as

$$\sigma_X = \int \frac{d\omega_1}{\omega_1}\frac{d\omega_2}{\omega_2} n_\gamma(\omega_1)\, n_\gamma(\omega_2)\, \sigma^X_{\gamma\gamma}(\omega_1\omega_2)\,, \tag{10}$$

where $n_\gamma(\omega)$ represents the equivalent photon flux, and $\sigma^X_{\gamma\gamma}(\omega_1\omega_2)$ is the cross section for producing particle X via two-photon interactions. The latter can be determined through a result due to Low [92], which connects the formation cross section with the particle's two-photon decay width:

$$\sigma^X_{\gamma\gamma}(\omega_1\omega_2) = 8\pi^2(2J+1)\frac{\Gamma_{m_X\to\gamma\gamma}}{m_X}\,\delta\left(\omega_1\omega_2 - m_X^2\right). \tag{11}$$

Here, m_X and J represent the mass and spin of the final state, while $\Gamma_{m_X\to\gamma\gamma}$ denotes its two-photon decay width. A more comprehensive analysis of mesonic and exotic candidates for such processes, including states often omitted from standard treatments, was presented in Ref. [93].

A worthy application of this formalism was proposed in 1989, aimed at identifying the Higgs boson in ultra-peripheral LHC collisions [94]. Using Equations (10, 11) and assuming plausible Higgs parameters, we estimated a production cross section of approximately 1 nb [3]. This value is on par with Higgs production in hadronic processes but with significantly reduced background particle production. Later studies pointed out that direct $\gamma\gamma \to b\bar{b}$ processes exhibit substantially larger cross sections [95], presenting a serious challenge for isolating the Higgs signal. A more favorable scenarios for Higgs detection in UPCs have been discussed in subsequent works [96, 97]. Since the Higgs predominantly decays into $b\bar{b}$ pairs, distinguishing it from this background remains a major challenge. Ultimately, the Higgs boson was confirmed via hadronic channels at the LHC by the ATLAS and CMS collaborations [98, 99].

Exotic hadronic configurations such as multiquark states, including molecular structures like $(q\bar{q})(q\bar{q})$, glueballs composed of gluons (gg), and hybrid mesons involving a gluon $(q\bar{q}g)$, play a pivotal role in understanding meson spectroscopy [100]. Ultra-peripheral collisions (UPCs) provide a promising experimental setting to explore these unconventional resonances via their unusual $\gamma\gamma$ couplings and characteristic energy levels. Such investigations can test theoretical expectations regarding non-standard states [68–70].

The decay width for $\gamma\gamma$ interactions is particularly informative, as it reflects the net electric charge of the quark constituents. This property can help distinguish between quark-based resonances and glueball candidates, which lack valence quarks. Therefore, the absence of certain meson states in $\gamma\gamma$ fusion experiments may serve as strong evidence for their gluonic origin [68–70]. In UPC scenarios, glueballs are typically produced through quark-antiquark annihilation into gluon pairs, whereas conventional mesons with $q\bar{q}$ structure are generated through direct photon-photon interactions.

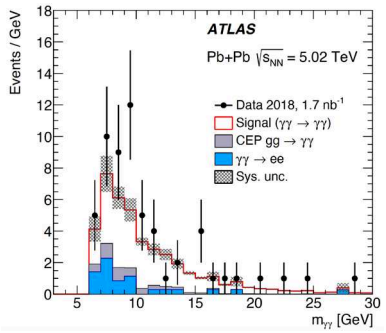

Figure 5. Light-by-light events obtained at the ATLAS detector [88].

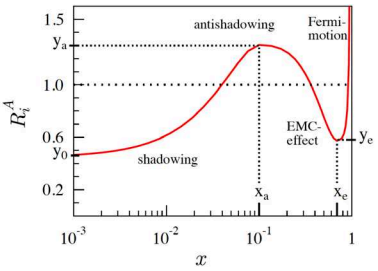

Figure 6. Medium effect dependence with the momentum fraction x.

8 Parton distribution functions

The study of vector meson production, such as for J/ψ and $\Upsilon(1s)$, can be addressed using Eq. (1), and early theoretical and experimental investigations were reported in Refs. [101–106]. In 2001, it was proposed [107] that coherent photoproduction of vector mesons could be utilized to probe the generalized parton distributions (GPDs) in nuclei, denoted $F_A(x, Q^2)$. This approach builds upon the formalism developed in Ref. [108], with the production cross section near zero momentum transfer given by

$$\left.\frac{d\sigma^{\gamma A\to VA}}{dt}\right|_{t=0} = \frac{16\pi\alpha_s^2(Q^2)\Gamma_{ee}}{3\alpha M_V^5}\left[xF_A(x,Q^2)\right]^2, \tag{12}$$

where $\alpha_s(Q^2)$ is the strong coupling constant evaluated at a pQCD scale $Q^2 = W_{\gamma g}^2$. Here, M_V is the mass of the produced vector meson, Γ_{ee} is its partial width for decay into e^+e^-, and $x = M_V^2/W_{\gamma p}^2$ corresponds to the gluon momentum fraction.

The nuclear parton distribution function (PDF), $F_a^A(\mathbf{r}, x, Q^2)$, describes the spatial and momentum distribution of a parton species a within a nucleus A, and can be represented as a convolution:

$$F_a^A(\mathbf{r}, x, Q^2) = R_a^A(\mathbf{r}, x, Q^2) \cdot f_a(x, Q^2),$$

where R_a^A encodes the nuclear modification, and $f_a(x, Q^2)$ denotes the parton distribution in a free nucleon [109]. The spatial coordinate $\mathbf{r}$ identifies the nucleon's position inside the nucleus. Different regions of Bjorken-x exhibit distinct nuclear effects. At small values ($x < 0.04$), parton densities are reduced relative to the nucleon baseline, a phenomenon known as shadowing, where $R_a^A < 1$ (see Figure 6). In the intermediate range $0.04 < x < 0.3$, the opposite behavior—antishadowing—occurs with $R_a^A > 1$. Between $0.3 < x < 0.8$, the EMC effect is dominant, and at large $x > 0.8$, enhancement arises due to nucleon Fermi motion. Each of these modifications reflects different physical mechanisms affecting parton distributions in the nuclear environment. In Ref. [109], we analyzed how different gluon parton distribution functions (PDFs) affect the production of vector mesons such as J/ψ and $\Upsilon(1s)$ in ultra-peripheral collisions. In particular, we distinguished between two dominant mechanisms in UPCs involving pPb and PbPb systems: the "direct" and "resolved" channels. The direct mechanism involves a photon interacting coherently with the nucleus, while the resolved process involves the photon fluctuating into a partonic configuration, typically a $q\bar{q}$ pair, which subsequently scatters off the nucleus.

At leading order, the direct channel is controlled by the gluon content of the nucleus, which is poorly constrained at small momentum fractions x (see Figure 8). In contrast, the

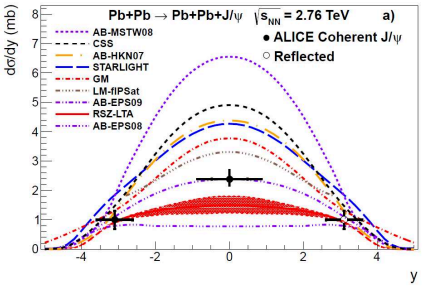

Figure 7. Rapidity y distribution of J/Ψ production in UPCs at the LHC. Different Parton Distribution Functions (PDFs) are tested [110].

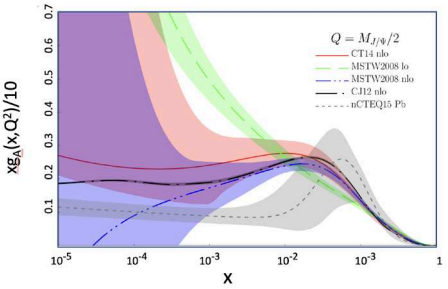

Figure 8. Compilation of gluon distribution functions depending on the momentum fraction x. Large error bands are evident.

resolved channel is sensitive to parton distributions in both the nucleus and the photon, including light quarks and gluons. Since vector meson production in UPCs depends quadratically on the gluon density, these processes provide enhanced sensitivity to the underlying nuclear gluon distributions, impacting both total and differential observables such as rapidity spectra [107, 109]. Our earliest predictions for J/ψ production, using nuclear gluon PDFs that incorporate shadowing effects [109], were found to be in excellent agreement with measurements performed by the ALICE collaboration [110–113], as shown in Figure 7. These findings support the use of J/ψ and Υ photoproduction in UPCs as a sensitive tool for probing gluon shadowing at very small x values, specifically in the regime $x < 10^{-3}$.

Currently, a widely supported view is that the resolved photon components play a crucial role in vector meson photoproduction within UPCs. Multiple studies [114–118] have emphasized the significant impact of hadronic fluctuations of the photon, especially in light meson production, and the relevance of leading-twist nuclear shadowing in $q\bar{q}$ photoproduction off heavy nuclei.

9 Perspectives

Ideas that first emerged during the 1980s and 1990s have since matured into a rich area of exploration at modern relativistic colliders. Ultra-peripheral collisions (UPCs) have revealed an array of surprising phenomena, such as the excitation of double giant resonances, production and investigation of anti-atoms, beam losses resulting from electron capture, light-by-light scattering, constraints on parton distribution functions (PDFs), and opportunities to probe physics beyond the Standard Model. These collisions could, in principle, enable the detection of processes like $\gamma\gamma \rightarrow$ graviton [119] or the production of axion-like particles [89, 90]. Whether such discoveries are feasible remains an open question, dependent on advancements in beam dynamics, accelerator performance, and innovative detector technologies.

Should searches at CERN continue to yield no evidence for supersymmetric particles, the focus may shift toward alternative strategies. These include refining precision calculations and experimental measurements, probing unconventional mesonic states, or further investigating how the nuclear medium influences parton distributions within hadrons.

Acknowledgments. This work was partially supported by the U.S. DOE grant DE-FG02-08ER41533, and the ExtreMe Matter Institute EMMI at the GSI Helmholtzzentrum für Schwerionenforschung, Darmstadt, Germany.

References

[1] E. Fermi, Zeit. Phys. **29**, 315 (1924); E. Fermi, Nuovo Cimento **2**, 143 (1925).
[2] C.A. Bertulani and G. Baur, Nucl. Phys. A **442**, 739 (1985).
[3] G. Baur and C.A. Bertulani, Physics Reports **163**, 299 (1988).
[4] C.A. Bertulani, S. Klein and J. Nystrand, Annu. Rev. Nucl. Part. Sci. **55**, 271 (2005).
[5] G. Baur, C. Bertulani and H. Rebel, Nucl. Phys. A **459**, 188 (1986).
[6] T. Motobayashi, et al., Phys. Rev. Lett. **73**, 2680 (1994).
[7] P. Navrátil, C.A. Bertulani, E. Caurier, Phys. Lett. B **634**, 191 (2006); PRC **73**, 065801 (2006).
[8] P. Descouvemont, D. Baye, Nuclear Phys. A **567**, 341 (1994).
[9] H. Esbensen, G.F. Bertsch, and K. Snover, Phys. Rev. Lett. **94**, 042502 (2005).
[10] M. Gai, Phys. Rev. Lett. **96**, 159201 (2006).
[11] E.G. Adelberger et al., Rev. Mod. Phys. **83**, 195 (2011).
[12] F.J. Vaughn, R.A. Chalmers, D. Kohler, L.F. Chase, Phys. Rev. C **2**, 1657 (1970).
[13] B.W. Filippone, A.J. Elwyn, C.N. Davids, D.D. Koetke, Phys. Rev. C **28**, 2222 (1983).
[14] L.T. Baby, et al., Phys. Rev. Lett. **90**, 022501 (2003).
[15] A.R. Junghans, et al., Phys. Rev. C **68**, 065803 (2003).
[16] N. Iwasa, et al., Phys. Rev. Lett. **83**, 2910 (1999).
[17] B.Davids, et al., Phys. Rev. Lett. **86**, 2750 (2001).
[18] F. Schümann, et al, Phys. Rev. Lett. **90**, 232501 (2003).
[19] R.W. Kavanagh, T.A. Tombrello, et al., Bull. Am. Phys. Soc. **14**, 1209 (169).
[20] S. Polikanov, et al., Z. Phys. A **350**, 221 (1994).
[21] P. Armbruster, et al., Z. Phys. A **355**, 191 (1996).
[22] T. Rubehn, et al., Z. Phys. A **353**, 197 (1995).
[23] T. Aumann, et al., Nuclear Phys. A **599**, 321 (1996).
[24] T. Aumann, C.A. Bertulani and K. Suemmerer, Phys. Rev. C **51**, 416 (1995).
[25] C.A. Bertulani, Phys. Rev. C **108**, 054602 (2023).
[26] T. Aumann, K. Suemmerer, C.A. Bertulani and J.V. Kratz, Nucl. Phys. A **599**, 321 (1996).
[27] G. Baur and C.A. Bertulani, Nucl. Phys. A **458**, 725 (1986).
[28] T. Aumann, K. Boretzky, J. Stroth, et al., Acta Physica Polonica. B **1**, 375 (1997).
[29] C.A. Bertulani, Y. Kucuk and R. Lozeva, Phys. Rev. Lett. **124**, 132301 (2020).
[30] I. Stetcu, et al., Phys. Rev. Lett. **114**, 012701 (2015).
[31] A.J. Baltz, C. Chasman and S.N. White Nucl. Inst. Meth. Phys. Res. A **41**, 1 (1998).
[32] Spencer R. Klein, Nucl. Inst. meth. Phys. **459**, 1 (2001).
[33] G. Baur and C.A. Bertulani, Phys. Lett. B **174**, 23 (1986).
[34] G. Baur and C.A. Bertulani, Phys. Rev. C **34**, 1654 (1986).
[35] R. Schmidt, et al., Phys. Rev. Lett. **70**, 1767 (1993).
[36] J. Ritman, et al Phys. Rev. Lett. **70**, 533 (1993).
[37] H. Emling, Prog. Part. Nucl. Phys. **33**, 729 (1994).
[38] T. Aumann, P.F. Bortignon and H. Emling, Ann. Rev. Nucl. Part. Sci. **48**, 351 (1998).
[39] C.A. Bertulani and G. Baur, Physics Today **47**, 22 (1994).
[40] C.A. Bertulani and V. Ponomarev, Phys. Reports **321**, 139 (1999).
[41] W.H. Furry and J.F. Carlson, Phys. Rev. **44**, 238 (1933).
[42] H.A. Bethe, Proc. Cambridge Philos. Soc. **30**, 524 (1934).
[43] H.J. Bhabha, Proc. R. Soc. London Ser. A **152**, 559 (1935).
[44] Y. Nishina, S. Tomonaga and H. Tamaki, Sci. Pap. Phys. Math. Res. Jpn **24**, 137 (1934).
[45] Y. Nishina, S. Tomonaga and M. Kobayashi, Sci. Pap. Inst. Phys. Chem. Res. **27**, 137 (1935).
[46] G. Racah, Nuovo Cimento **14**, 93 (1937).
[47] G. Baur and C.A. Bertulani, Nucl. Phys. A **505**, 835 (1989).
[48] G. Baur, K. Hencken, D. Trautmann, S. Sadovsky, Y. Kharlov, Phys. Reports **364**, 359 (2002).

[49] K. Hencken, D. Trautmann, G. Baur, Phys. Rev. A **51**, 998 (1995).
[50] G. Baur, K. Hencken and D. Trautmann Phys. Reports **453**, 1 (2007).
[51] A.J. Baltz et al. Phys. Reports **458**, 1 (2008).
[52] J. Adams et al. (STAR Collaboration), Phys. Rev. C **70**, 031902 (2004).
[53] W. Adam, et al., Phys. Lett. B **797**, 303 (2008).
[54] G. Baur and C.A. Bertulani, Phys. Rev. C **35**, 836 (1987).
[55] C.A. Bertulani and G. Baur, Z. Phys. A **330**, 77 (1988).
[56] C.A. Bertulani C A and G. Baur, Phys. Rev. D **58** 034005 (1998).
[57] C.A. Bertulani and M. Ellermann, Phys. Rev. C **81** 044910 (2010).
[58] C. Munger and S. Brodsky, Phys. Rev. D **49**, 3228 (1994).
[59] G. Baur, et al, Phys. Lett. B **368**, 3 (1996).
[60] Malcolm W. Browne, The New York Times, January 5 (1996).
[61] G. Blanford et al., Phys. Rev. Lett. **80**, 3037 (1998).
[62] C.A. Bertulani and D. Dolci, Nucl. Phys. A **683**, 635 (2001).
[63] E.S. Reich, Nature News **11**, 17 (2010).
[64] L. Grossman Phys. Rev. Focus **26** (2010).
[65] H. Agakishiev, et al, Nature, **473**, 353 (2011).
[66] S.R. Klein, Phys. Rev.: Accelerators and Beams **17**, 121003 (2014).
[67] J.M. Schaumann, et al. , Phys. Rev.: Accelerators and Beams **23**, 121003 (2020).
[68] C.A. Bertulani and F.S. Navarra Nucl. Phys. A **703**, 861 (2002).
[69] B.D. Moreira, C.A. Bertulani, V.P. Goncalves and F. S. Navarra Phys. Rev. D **94**, 094024 (2016).
[70] C.A. Bertulani, V.P. Goncalves, B.D. Moreira and F.S. Navarra Eur. Phys. J. **137**, 06019 (2017).
[71] R. Fariello, D. Bhandari, C. A. Bertulani and F. S. Navarra, Phys. Rev. C **108**, 044901 (2023).
[72] M. Deutsch, Proc. Am. Acad. Art. Sci. **82**, 331(1953).
[73] V.W. Hughes, D.W. McColm, K. Ziock, R. Prepost, Phys. Rev. Lett. **5**, 63 (1960).
[74] D.B. Cassidy, A.P. Mills, Nat.(Lond.) **449**, 195 (2007).
[75] P.J. Fox, S. Jindariani, V. Shiltsev, arXiv:2203.07144 (2022).
[76] V.W. Hughes, B. Maglic, Bull. Am. Phys. Soc. **16**, 65 (1971).
[77] F. Ginzburg, U.D. Jentschura,et al., Phys. Rev. C **58** 3565 (1998).
[78] P.A. Krachkov, and A.I. Milstein, Nucl. Phys. A **971**, 71 (2018).
[79] C. Azevedo, V. P. Gonçalves, and B. D. Moreira, Phys. Rev. C **101**, 024914 (2020).
[80] R. Francener, V. P. Gonçalves, and B. D. Moreira, Eur. Phys. J. A **58**, 35 (2022).
[81] C. A. Bertulani, D. Bhandari, F.S. Navarra, Eur. Phys. J. A **60**, 43 (2024).
[82] David d'Enterria and Hua-Sheng Shao, Phys. Lett. B **842**, 137960 (2023).
[83] D. d'Enterria and G.G. da Silveira, Phys. Rev. Lett. **111**, 080405 (2013).
[84] M. Kłusek-Gawenda, P. Lebiedowicz, and A. Szczurek, Phys. Rev. C **93**, 044907 (2016).
[85] P. Lebiedowicz and A. Szczurek, Phys. Lett. B **772**, 330 (2017).
[86] M. Klusek-Gawenda, R. McNulty,, R. Schicker and A. Szczurek, Phys. Rev. D **99**, 093013 (2019).
[87] P. Jucha, M. Klusek-Gawenda and A. Szczurek, Phys. Rev. D **109**, 014004 (2024).
[88] G. Aaboud, et al., The ATLAS collaboration, Nature Physics **13**, 852 (2017).
[89] V. Gonçalves and W. Sauter Phys. Lett. B **811**, 135981 (2020).
[90] V.P. Gonçalves, D.E. Martins and M. Rangel, Eur. Phys. J. C **81**, 522 (2021).
[91] L. Schoeffel, et al., Nucl. Phys. **1005**, 121840 (2021).
[92] F.E. Low F E Phys. Rev. **120**, 582 (1960).
[93] C.A. Bertulani, Phys. Rev. C **79** 047901 (2009).
[94] E. Papageorgiu, Phys. Rev. D **40**, 92 (1989).
[95] M. Drees, J. Ellis, D. Zeppenfeld, Phys. Lett. B **223**, 454 (1989).
[96] David d'Enterria and Jean-Philippe Lansberg, Phys. Rev. D **81**, 014004 (2010).
[97] David d'Enterria, Daniel E. Martins, and Patricia Rebello Teles, Phys. Rev. D **101**, 033009 (2020).
[98] ATLAS Collaboration, Phys. Lett. B **716**, 1 (2012).

[99] CMS Collaboration, Phys. Lett. B **716**, 30 (2012).
[100] W-M Yao, et al., J. Phys. G **33**, 1 (2006).
[101] Spencer R. Klein and Joakim Nystrand, Phys. Rev. C **60**, 014903 (1999).
[102] Spencer R. Klein and Joakim Nystrand, Phys. Rev. Lett. **84**, 2330 (2000).
[103] Anthony J. Baltz, Spencer R. Klein, and Joakim Nystrand, Phys. Rev. Lett. **89**, 012301 (2002).
[104] C. Adler et al. (STAR Collaboration), Phys. Rev. Lett. **89**, 272302 (2002).
[105] B. I. Abelev et al. (STAR Collaboration), Phys. Rev. C **77**, 034910 (2008).
[106] PHENIX Collaboration, Phys. Lett. B **679**, 321 (2009).
[107] V.P. Goncalves and C.A. Bertulani, Phys. Rev. C **65**, 054905 (2002).
[108] L. L. Frankfurt, W. Koepf and M. Strikman, Phys. Rev. D **57**, (1998) 512
[109] A. Adeluyi and C.A. Bertulani, Phys. Rev. C **84**, 024916 (2011); Phys. Rev. C **85**, 044904 (2012).
[110] B. Abelev, et al. (ALICE Collaboration), Phys. Lett. B **718**, 1273 (2013).
[111] J. D. Tapia Takaki; ALICE Collaboration, AIP Conf. Proc. **1523**, 221 (2013).
[112] A. Abelev, et al., (ALICE Collaboration) Eur. Phys. J. C **73**, 2617 (2013).
[113] D. De Gruttola D (ALICE Collaboration), Nucl. Phys. A **926**, 136 (2014).
[114] V. Guzey, E. Kryshen, M. Strikman, M. Zhalov, Phys. Lett. B **726**, 290 (2013).
[115] V. Guzey, M. Strikman, and M. Zhalov, Phys. Rev. C **95**, 025204 (2017).
[116] V.P. Gonçalves, F.S. Navarra, and D. Spiering, Phys. Lett. B **791**, 299 (2019).
[117] V. P. Gonçalves, D. E. Martins, and C. R. Sena, Eur. Phys. J. A **57**, 82 (2021).
[118] Yuri V. Kovchegov, Huachen Sun, Zhoudunming Tu, [hep-ph] arXiv:2311.12208 (2023).
[119] S. Ahern, J.W. Norbury and W. Poyser, Phys. Rev. D **62**, 116001 (2000).